Lattice-type-dependent momentum-exchange method for moving boundaries

Binghai Wen,[1,2,4] Huabing Li,[3] Chaoying Zhang,[2,*] and Haiping Fang[1,4]

[1]*Shanghai Institute of Applied Physics, Chinese Academy of Sciences, Shanghai 201800, China*

[2]*College of Computer Science and Information Engineering, Guangxi Normal University, Guilin 541004, China*

[3]*Department of Information Material Science and Engineering, Guilin University of Electronic Technology, Guilin 541004, China*

[4]*Graduate School of the Chinese Academy of Sciences, Beijing 100080, China*

(Received 15 June 2011; revised manuscript received 12 November 2011; published 6 January 2012)

The conventional momentum-exchange method (CME) is verified to be accurate for the stationary boundary by Mei *et al.* [Phys. Rev. E **65**, 041203 (2002)], but it might be inaccurate when the boundary is moving in the lattice Boltzmann simulations. A lattice-type-dependent momentum-exchange method (LME) is presented to evaluate the hydrodynamic force on moving boundaries, in which the additional momenta induced by the type-changing lattices are well considered. LME preserves the superior features of CME, such as reliability, simplicity, and parallelism. Without any interpolation and integration, the algorithm is independent of boundary geometries, and therefore, efficient in computation and easy to be implemented in both two and three dimensions. A series of cylinder sedimentations are simulated to illustrate the accuracy and robustness of LME, and the results are in excellent agreement with those by the arbitrary Lagrangian-Eulerian technique (ALE). The lateral migrations of a particle are also investigated in the simulations of a neutrally buoyant cylinder in a Poiseuille flow, and consistent with the Segré-Silberberg effect.

DOI: 10.1103/PhysRevE.85.016704 PACS number(s): 47.11.−j, 47.10.−g, 05.20.Dd

I. INTRODUCTION

Over the past two decades, the lattice Boltzmann equation [1–3] has developed into an alternative and promising numerical scheme for simulating complex fluid flows [4–6] and is particularly successful in applications involving interfacial dynamics [7–9], microflows [10–12], multiphase flows [13,14], magnetohydrodynamics [15–17], and complex boundaries [18–21]. In the numerical stimulation of complex fluid-solid flow [22–27], force evaluation plays an essential role to depict exactly the behavior of the moving particle in the carrier fluid. Many efforts have been contributed to develop and improve the schemes of calculating the fluid-solid forces, and a number of algorithms have been proposed. Up to now, the two most commonly used schemes are the momentum-exchange method and the stress-integration method, which have been already successfully used to simulate the problems with fluid-solid interactions.

A. Force evaluation based on momentum-exchange method

In the numerical simulations of particulate suspensions, Ladd created the original momentum-exchange model for evaluating hydrodynamic interactions [22,23]. His pioneer works promoted the lattice Boltzmann method to become a popular tool in simulating fluid-solid interaction problems. The solid particle, in Ladd's method, was defined by a boundary surface and all lattices, both inside and outside of the solid particle, were treated as fluid lattices in an identical fashion. Ladd laid the particle boundary discretely and approximately at the middle of the link between a solid node and a fluid node, namely a fluid-solid link. A momentum item based on the boundary velocity was added to the distribution functions which were bounced back from the particle boundary, and the momentum-exchange occurred during the streaming step. As a result, the force exerted on the solid particle by the fluid was obtained by summing the momentum transfers over all the fluid-solid links. In Ladd's method, the population rearrangements of the distribution functions can only be made among the pairs of the opposite velocities crossing the particle boundary.

Aidun *et al.* [24,25] improved Ladd's model by directly representing the solid particle without fluid inside. Arranging the particle boundary approximately at one-half of the fluid-solid links the same as Ladd's method, he extended the halfway bounce-back rule by adding the momentum item based on the boundary velocity to the distribution function bounced back from the particle boundary. An additional term was introduced in order to conserve the mass of the boundary nodes. The particle boundary, therefore, can be treated as an impermeable surface in Aidun's method. Another improvement in his method is that, for moving solid particles, the momenta of the covered and uncovered nodes were involved in the force evaluation, but their effect was not investigated in detail. Later, Behrend [28] proposed a relaxed bounce-back method by combining bounce-back with halfway bounce-back in order to avoid distribution functions being trapped between two boundary nodes. Lorenz *et al.* [29] investigated the effects of the Lees-Edwards boundary condition and added a correction term to Ladd's and Aidun's methods in order to improve the accuracy.

Mei *et al.* [30] introduced the curved boundary condition [31–33] into the momentum-exchange method so that the particle geometry could be accurately represented on the grid level. The distribution functions bounced back from the solid boundary and the force evaluation were carried out on the real geometry of the solid particle instead of the previous stepping edges, and the simulation accuracy was improved consequently.

*zhangcy@gxnu.edu.cn

Based on these momentum-exchange methods mentioned above, Ladd [7,22,23] and Aidun [24,25] simulated the particle suspension in fluid and provided some detailed analyses. Ladd [34] studied hydrodynamic screening in sedimentation suspensions of non-Brownian spheres. Qi *et al.* [26,35] simulated the nonspherical particle in nonzero Reynolds number flow and the behaviors of three-dimensional spheroidal particles in Couette flows. Wan *et al.* [36] studied the sedimentation of a single charged circular cylinder in Newtonian fluid. Zhang *et al.* [37,38] simulated a charged elliptic cylinder and a charged elastic dumbbell in Newtonian fluid, respectively. Basagaoglu *et al.* [39] simulated the accelerated transport of dense inert particles flows in smooth-walled and rough-walled narrow channels in low Reynolds number. In 2002, Mei *et al.* [30] compared the momentum-exchange method with the stress-integration method proposed by He and Doolen [40] and concluded that the former was simpler, more accurate, and robust.

B. Force evaluation based on stress-integration method

Another usual scheme for evaluating hydrodynamic forces is the stress-integration method. He and Doolen [40] proposed the interpolation-supplemented lattice Boltzmann equation on a polar-coordinate grid system near the cylinder surface and evaluated the force by integrating the total stresses on the surface of the cylinder:

$$\mathbf{F} = \int_{\partial\Omega} dA\mathbf{n} \cdot [-pI + \rho v(\nabla \cdot \mathbf{u} + \mathbf{u} \cdot \nabla)], \tag{1}$$

where $\partial\Omega$ is the particle's boundary, $\mathbf{n}$ the unit outward normal vector, p the pressure, and I the unit matrix. With the irregular grid, more lattices can be placed near the body to yield a reliable velocity gradient. However, the accuracy would be degraded due to the data conversion from the Cartesian grid to the curvilinear coordinate.

According to the method proposed by Inamuro *et al.* [41], the stress tensor can be calculated as follows:

$$\sigma_{ij} = -\frac{1}{6\tau}\rho\delta_{ij} - \left(1 - \frac{1}{2\tau}\right)\sum (e_{\alpha i} - u_i)(e_{\alpha j} - u_j) f_\alpha, \tag{2}$$

where δ_{ij} is the Kronecker delta function and $i, j = x, y$. This process avoided using velocity gradients to calculate the stress tensor. With S denoting a closed surface apart from the cylinder, the hydrodynamic force could be computed by integrating the stress tensor and momentum flux on S:

$$\mathbf{F} = \int_S \{\sigma \cdot \mathbf{n} - \rho\mathbf{u}[(\mathbf{u} - \mathbf{V}) \cdot \mathbf{n}]\} \cdot ds, \tag{3}$$

where $\mathbf{n}$ is the unit outward normal vector of the boundary and $\mathbf{V}$ is the velocity of the mass center of the solid particle. The integral of Eq. (3) was approximated by the numerical quadrature of 400 points. Since the circular surface was represented by the square grids, the diameter of S was chosen to be 1.16 times the cylinder diameter. As a result, this method is approximate and very limited in use.

Based on the method presented by Inamuro *et al.* [41], Li *et al.* [42] applied the curved boundary condition to stress tensor integration and proposed an extrapolation scheme to obtain the distribution functions of the virtual points which are evenly scattered on the particle boundary. The fluid-solid interaction was also computed by Eqs. (2) and (3).

Using these stress-integration methods, He and Doolen [40] simulated two-dimensional flow around a circular cylinder. Inamuro *et al.* [41] studied the motions of single and two-line cylinders in the flow. Xia *et al.* [43] investigated the sedimentation of an elliptical particle. In 2004, Li *et al.* [42] compared a series of cylinder sedimentations in Newtonian fluid with those done by the arbitrary Lagrangian-Eulerian technique [44] and reached good agreement. They concluded that the stress-integration method obtained better accuracy than the momentum-exchange method.

C. Comparison of the two methods for force evaluations

The stress-integration method [42] with the curved boundary condition gets some good results for the force evaluation of moving boundaries in the lattice Boltzmann simulations. However, the distribution functions of the virtual points on the boundary can only be obtained by complex extrapolation schemes. So the stress-integration method not only is more noisy and unstable, but also causes much heavier computing loads than the momentum-exchange method. Furthermore, as the integration is carried out on the whole boundary, the stress-integration method encounters especial troubles on the boundary with complex geometries. For example, how to distribute the virtual points equably on the curved surface is not trivial work, especially in three dimensions.

On the contrary, the momentum-exchange method is based directly on the distribution functions, and the fluid-solid interaction can be calculated simply by the summation of the momenta passing through the boundary without any interpolation or extrapolation procedure. Since the momentum density is immediately defined as the product of the distribution function and its corresponding discrete velocity, the implementation of the algorithm is very simple. The computing locality and the consequent superior parallelism of the lattice Boltzmann method are fully preserved in the momentum-exchange method. Furthermore, the momentum-exchange method is independent of the boundary geometry, and thus easily applied to the simulations with complex geometries in both two and three dimensions.

In both Ladd's and Aidun's methods, the particle boundary is set at the middle of the fluid-solid links; the real particle boundary is replaced by a series of stepping edges. Consequently, the force evaluation based on these methods has to be approximate even if some correction terms are considered [29]. In the method proposed by Mei *et al.* [30], the particle boundary can be exactly represented by using the curved boundary condition, thus the approximate result from the zigzag boundary is improved. Mei *et al.* verified the conventional momentum exchange [30] by several test cases with stationary boundaries, including pressure-driven channel flow, uniform flow past a column of cylinders, flow past a cylinder, flow past a sphere, and so on, and concluded that it is simple, accurate, and robust in computing hydrodynamics forces on curved boundaries. The accuracy of the momentum-exchange method for the problems involving moving boundaries was not investigated. In fact, the conventional momentum-exchange

method [30] is inaccurate when it is applied to the cases with moving boundaries, which will be illustrated in the following sections (as shown in Figs. 3 and 5–8).

Consequently, it is meaningful to develop an improved momentum-exchange method, which not only preserves the original merits, but also can be used to evaluate accurately the hydrodynamic force on moving boundary.

D. Scope of the present work

The paper is organized as follows. In Secs. II and III we briefly describe the lattice Boltzmann method and the curved boundary conditions. Section IV is devoted to a description of the lattice-type-dependent momentum-exchange method. The numerical simulations with the lattice-type-dependent momentum-exchange method and their comparisons with the published results are presented in detail in Sec. V. Section VI concludes the paper.

II. LATTICE BOLTZMANN METHOD

The lattice Boltzmann equation (4) with a single relaxation time approximation (SRT) is given by

$$\frac{\partial f_i}{\partial t} + \mathbf{e}_i \cdot \nabla f_i = -\frac{1}{\tau}\left(f_i - f_i^{(\mathrm{eq})}\right), \quad (i = 0,1,2,\ldots,N-1), \tag{4}$$

where $\mathbf{e}_i$ is a discrete velocity vector, f_i the particle distribution function with the velocity $\mathbf{e}_i$, $f_i^{(\mathrm{eq})}$ the corresponding equilibrium distribution function, N the number of the different velocities in the model, and τ the relaxation time. Equation (4) is then discretized, in space $\mathbf{x}$ and time t, into

$$f_i(\mathbf{x}+\mathbf{e}_i\delta t, t+\delta t) - f_i(\mathbf{x},t) = -\frac{1}{\tau}\left[f_i(\mathbf{x},t) - f_i^{(\mathrm{eq})}(\mathbf{x},t)\right], \tag{5}$$

where δt is the time step. In the model on a square lattice in two dimensions (D2Q9), the discrete velocity set is given by $\mathbf{e} = \{(0,0),(1,0),(0,1),(-1,0),(0,-1),(1,1),(-1,1),(-1,-1),(1,-1)\}$. The particle equilibrium distribution function can be written as

$$f_i^{(\mathrm{eq})} = \rho\omega_i\left[1 + \frac{3}{c^2}(\mathbf{e}_i\cdot\mathbf{u}) + \frac{9}{2c^4}(\mathbf{e}_i\cdot\mathbf{u})^2 - \frac{3}{2c^2}\mathbf{u}^2\right], \tag{6}$$

where $\omega_0 = 4/9$, $\omega_{1,2,3,4} = 1/9$, $\omega_{5,6,7,8} = 1/36$. Based on this equilibrium distribution function and applying the Chapman-Enskog expansion, the continuity equation and the Navier-Stokes equations can be recovered at the second-order approximation from Eq. (2) if the density variation is sufficiently small. The macroscopic physics quantities' density and momentum density are defined by the distribution function f_i:

$$\rho = \sum_i f_i, \quad \rho\mathbf{u} = \sum_i f_i\mathbf{e}_i. \tag{7}$$

The lattice Boltzmann method applies two essential steps, namely collision and streaming, to reveal the flow phenomena at the mesoscopic scale. Hence, the corresponding computations of Eq. (5) are performed as

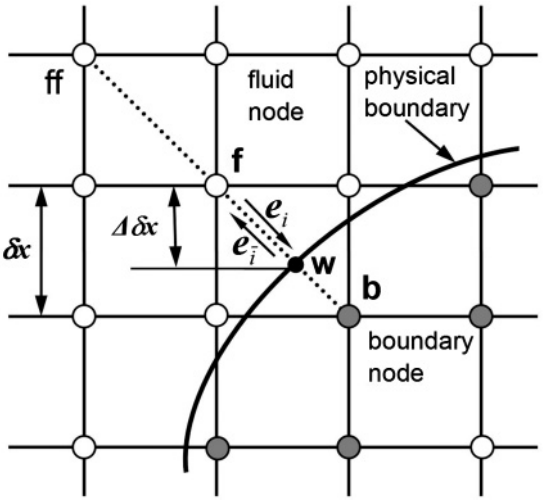

FIG. 1. Lay out of the curved boundary.

$$\text{Collision: } \tilde{f}_i(\mathbf{x},t) - f_i(\mathbf{x},t) = -\frac{1}{\tau}\left[f_i(\mathbf{x},t) - f_i^{(\mathrm{eq})}(\mathbf{x},t)\right], \tag{8}$$

$$\text{Streaming: } f_i(\mathbf{x}+\mathbf{e}_i\delta x, t+\delta t) = \tilde{f}_i(\mathbf{x},t), \tag{9}$$

where f_i and $\tilde{f}_i$ denote precollision and postcollision states of the particle distribution functions, respectively. The dominant part of the computations, namely the collision step, is completely local, so the discrete equations are natural to parallelize.

III. BOUNDARY CONDITION FOR COMPLEX GEOMETRY

Filippova and Hanel [31] presented firstly a curved boundary treatment for the lattice Boltzmann model. Their method considered a boundary lying between the solid and the fluid nodes denoted, respectively, by $\mathbf{x}_b$ and $\mathbf{x}_f$ as shown in Fig. 1. The physical boundary intersects the fluid-solid link between $\mathbf{x}_b$ and $\mathbf{x}_f$ at the point $\mathbf{x}_w$. $\mathbf{e}_i$ and $\mathbf{e}_{\bar{i}}$ stand for directions opposite to each other, which are defined as $\mathbf{e}_i = \mathbf{x}_b - \mathbf{x}_f$ and $\mathbf{e}_{\bar{i}} = -\mathbf{e}_i$, respectively. The lattice spacing is $\delta x = 1$. The fraction of the intersected link in the fluid region is Δ, that is,

$$\mathbf{\Delta} = |\mathbf{x}_f - \mathbf{x}_w|/|\mathbf{x}_f - \mathbf{x}_b|, \quad 0 \leqslant \mathbf{\Delta} \leqslant 1. \tag{10}$$

After the collision step, the distribution function $\tilde{f}_{\bar{i}}(\mathbf{x}_b,t)$ must be computed to finish the streaming step. To obtain a second-order scheme for "slow flow," Filipova and Hanel proposed using the following linear interpolation:

$$\tilde{f}_{\bar{i}}(\mathbf{x}_b,t) = (1-\chi)\tilde{f}_i(\mathbf{x}_f,t) + \chi f_i^{(*)}(\mathbf{x}_b,t) - 2\omega_i\rho\frac{3}{c^2}(\mathbf{e}_i\cdot\mathbf{u}_w), \tag{11}$$

where $\mathbf{u}_w$ is the velocity at $\mathbf{x}_w$, χ is the weighting factor, and $f_i^{(*)}$ is a fictitious equilibrium distribution function given by

$$f_i^{(*)}(\mathbf{x}_b,t) = \rho\varpi_i\left[1 + \frac{3}{c^2}\mathbf{e}_i\cdot\mathbf{u}_{bf} + \frac{9}{2c^4}(\mathbf{e}_i\cdot\mathbf{u}_f)^2 - \frac{3}{2c^2}\mathbf{u}_f^2\right], \tag{12}$$

where $\mathbf{u}_f = \mathbf{u}(\mathbf{x}_f,t)$ is the fluid velocity, and $\mathbf{u}_{bf}$ is the assumed velocity at $\mathbf{x}_b$. Then χ and $\mathbf{u}_{bf}$ are given by

$$\mathbf{u}_{bf} = \begin{cases} (\Delta-1)\mathbf{u}_f/\Delta, & \chi = (2\Delta-1)/\tau, \quad \text{for } \Delta \geqslant 0.5 \\ \mathbf{u}_f, & \chi = (2\Delta-1)/(\tau-1), \quad \text{for } \Delta \leqslant 0.5. \end{cases} \tag{13}$$

Mei *et al.* [32,33] improved the stability of the scheme by replacing Eq. (13) with

$$\mathbf{u}_{bf} = \begin{cases} (1-3/2\Delta)\mathbf{u}_f, & \chi = (2\Delta-1)/(\tau+0.5), \quad \text{for } \Delta \geqslant 0.5 \\ \mathbf{u}_{ff}, & \chi = (2\Delta-1)/(\tau-2), \quad \text{for } \Delta \leqslant 0.5. \end{cases} \tag{14}$$

where $\mathbf{u}_{ff}$ is the fluid velocity at fluid node ff shown in Fig. 1.

IV. LATTICE-TYPE-DEPENDENT MOMENTUM-EXCHANGE METHOD

A. Conventional momentum-exchange method

We analyze firstly how the momentum-exchange is implemented in the lattice Boltzmann method. According to the lattice Boltzmann equation, the momentum density is described by Eq. (7), which represents the momentum of the fluid in a lattice. On the other hand, the lattice's momentum in Eq. (7) can be interpreted as the sum of its eight momentum components based on the principle of vectors superposition. During the streaming step, the distribution function $\tilde{f}_i$ at site $\mathbf{x}$ will stream to its neighbor lattice at site $\mathbf{x}+\mathbf{e}_i$, and the momentum component $\mathbf{e}_i\tilde{f}_i$ will also transfer from the original lattice to the target lattice.

In the curved boundary condition [31–33], the distribution functions bounced back from the particle's surface are calculated by Eq. (11), in which the boundary positions between the solid and fluid nodes are under exact treatment. Taking the consistency into consideration, the bounced-back distribution functions and their corresponding momenta can be regarded as that streaming out of the solid nodes.

In the conventional momentum-exchange method [30], the momentum exchange between the fluid and the solid particle is obtained on the fluid-solid links. For a fluid-solid link associated with the velocity $\mathbf{e}_i$ with the direction from a fluid node to a solid node, the momentum $\mathbf{e}_i\tilde{f}_i$ goes into the solid particle and contributes a momentum increment to it. For the reverse direction, $\mathbf{e}_{\bar{i}}\tilde{f}_{\bar{i}}$ goes out of the solid particle and contributes a momentum decrement to it. So, the momentum-exchange value on the fluid-solid link, namely the force, can be written as [30,42]

$$\mathbf{F}(\mathbf{x}_b) = \mathbf{e}_i\tilde{f}_i(\mathbf{x}_f,t) - \mathbf{e}_{\bar{i}}\tilde{f}_{\bar{i}}(\mathbf{x}_b,t) = \mathbf{e}_i[\tilde{f}_i(\mathbf{x}_f,t) + \tilde{f}_{\bar{i}}(\mathbf{x}_b,t)], \tag{15}$$

where $\tilde{f}_{\bar{i}}(\mathbf{x}_b,t)$ is calculated by Eq. (11), $\boldsymbol{x}_f$ is a fluid node, $\boldsymbol{x}_b$ is a boundary node, i is the direction from $\boldsymbol{x}_f$ to $\boldsymbol{x}_b$, and $\bar{i}$ is the opposite direction. The total hydrodynamic force $\mathbf{F}_p$ and torque $\mathbf{T}_p$ acting on the solid particle are evaluated by

$$\mathbf{F}_p = \sum \mathbf{F}(\mathbf{x}_b), \tag{16}$$

and

$$\mathbf{T}_p = \sum (\mathbf{x}_b - R) \times \mathbf{F}(\mathbf{x}_b), \tag{17}$$

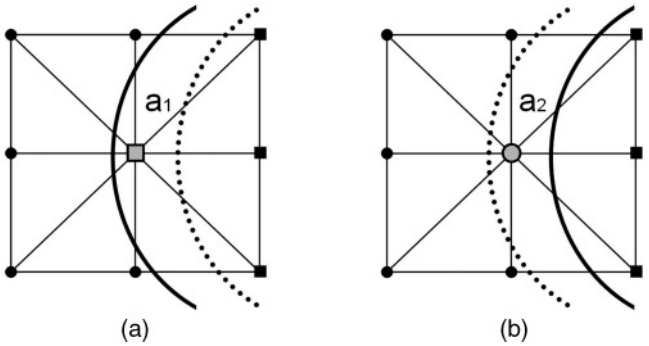

FIG. 2. The nodes' types are changed when the boundary moves from the dotted curve to the real curve. Circles denote the fluid and squares denote the particle. The shaded square a_1 in (a) represents a new solid node changed from a fluid node and the shaded circle a_2 in (b) represents a new fluid node changed from a solid node.

where R is the mass center of the solid particle, and the summation runs over all the fluid-solid links. It is clear that all momentum components used in the force evaluation are always on the fluid-solid links.

B. Lattice-type-dependent momentum-exchange method

For the stationary boundaries, the accuracy of the conventional momentum-exchange method was verified by Mei *et al.* [30]. However, when the solid particle moves in a lattice Boltzmann simulation, it may cover or uncover some lattices, which lead to the changes of the lattice types. In the conventional method, the momenta of the type-changing lattices are not well considered, and the corresponding influences on the hydrodynamic force evaluation are not investigated in detail yet. In this article, we take the momenta of the type-changing lattices into account, and establish the lattice-type-dependent momentum-exchange method based on the curved boundary condition.

It is obvious that each of the momentum components passing through the boundary will change the momentum of the solid particle. When the boundary shifts from the dotted curve to the real curve in a time step as shown in Fig. 2(a), the previous fluid node (a_1) is devoured by the solid particle and becomes a new solid node now. Each of its momentum components goes into the boundary and contributes a momentum increment to the solid particle. So, the impulse force caused by the node (a_1) can be written as

$$\mathbf{F}(\mathbf{x}_c) = \sum_i \mathbf{e}_i\tilde{f}_i(\mathbf{x}_c,t), \tag{18}$$

where $\mathbf{x}_c$ is the position of a lattice changing from fluid into solid and refers to the node (a_1) in Fig. 2(a).

In a similar way, when the boundary moves as shown in Fig. 2(b), the previous solid node (a_2) is uncovered and becomes a new fluid node. Each of its momentum components goes out of the boundary and contributes a momentum decrement to the solid particle. The impulse force caused by the node (a_2) can be written as

$$\mathbf{F}(\mathbf{x}_c) = -\sum_i \mathbf{e}_i\tilde{f}_i(\mathbf{x}_c,t), \tag{19}$$

where $\boldsymbol{x}_c$ is the position of a lattice changing from solid into fluid and refers to the node (a_2) in Fig. 2(b).

We add the momenta of the type-changing lattices into the conventional momentum-exchange method, and then the hydrodynamic force evaluation should include two parts for the moving boundary. One is carried out on the fluid-solid links as in the conventional method, and the other is obtained from the type-changing lattices with Eqs. (18) and (19). Consequently, the hydrodynamic force and torque exerted on the solid particle can be written as

$$\mathbf{F}_p = \sum \mathbf{F}(\mathbf{x}_b) + \sum \mathbf{F}(\mathbf{x}_c), \tag{20}$$

and

$$\mathbf{T}_p = \sum (\mathbf{x}_b - R) \times \mathbf{F}(\mathbf{x}_b) + \sum (\mathbf{x}_c - R) \times \mathbf{F}(\mathbf{x}_c), \tag{21}$$

where the summation of $\boldsymbol{x}_b$ runs over all the fluid-solid links and the summation of $\boldsymbol{x}_c$ on all type-changing lattices.

In order to prevent the impulse forces by Eqs. (18) and (19) from generating the new type-changing lattices in the same time step, the exertion of these forces can be postponed to the next time step. With Eqs. (18)–(21), we know that the force evaluation by the lattice-type-dependent method does not need to buffer any more data or iterate any more steps than the conventional method. So, the algorithm is efficient in both the time complexity and space complexity, and does not destroy the parallelism of the lattice Boltzmann method.

Because the lattice-type-dependent momentum-exchange method is only dependent on the existing distribution functions and independent of the collision step of the lattice Boltzmann equation, it can be combined with different curved boundary conditions and used in other lattice Boltzmann models, such as the multiple-relaxation-time (MRT) [45,46], the two-relaxation-time (TRT) [47], etc.

C. Distinction of the force evaluations

Figure 3 shows the hydrodynamic forces in the simulations in Sec. V, which are evaluated by the conventional momentum-exchange method (CME), lattice-type-dependent momentum-exchange method (LME), and arbitrary Lagrangian-Eulerian technique (ALE), respectively. It is clear that the result by LME is in excellent agreement with the benchmark from the arbitrary Lagrangian-Eulerian technique, and that from the conventional method deviates evidently from the others. This implies that the momenta of the type-changing lattices, which are ignored in the conventional method, are significant and the lattice-type-dependent momentum-exchange method reflects correctly the momentum-exchange between the solid particle and its surrounding fluid when the boundaries are moving.

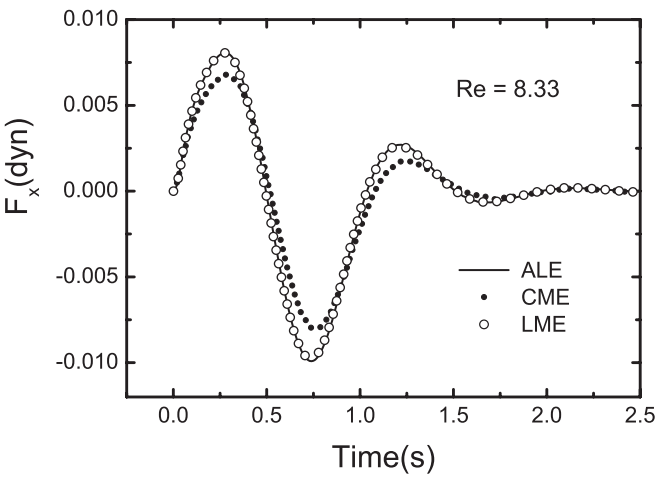

FIG. 3. Time-dependent particle force in the sedimentation simulation at Re = 8.33.

V. SIMULATION RESULTS AND DISCUSSION

The lattice Boltzmann method has been successfully applied to the simulations of particle suspensions, which play an important role in many industrial and biological situations [5,7]. In this section, we conduct some numerical simulations to verify the proposed method. Section V A investigates the accuracy of the lattice-type-dependent momentum-exchange method by comparing to the benchmarks from the arbitrary Lagrangian-Eulerian technique [44]. Section V B shows that the proposed method can correctly simulate the Segré-Silberberg effect [48].

A. Sedimentation of a circular cylinder in a vertical channel

The flow geometry is shown in Fig. 4. A circular cylinder is deployed away from the channel's central line in a static fluid of a vertical channel. Since the mass density of the cylinder is somewhat bigger than that of the fluid, it descends, rotates, and translates under gravitational force and hydrodynamic force. Finally, it reaches an equilibrium state in which the cylinder goes down at a constant velocity along with the central line. Hu *et al.* studied the issue extensively using the arbitrary Lagrangian-Eulerian technique [44,49]. In a previous paper [42], Li *et al.* used the stress-integration method to evaluate the hydrodynamic force on the circular cylinder and obtained good agreement with Hu's results. Although the conventional momentum-exchange method can describe roughly the dynamic behavior of the cylinder, there are some considerable discrepancies in velocities, angular velocities, and trajectories. In the present paper, we study the same issue by using the lattice Boltzmann method with the lattice-type-dependent momentum-exchange method.

The diameter of the cylinder is 0.1 cm and the channel width is 0.4 cm. The cylinder is released at 0.076 cm away

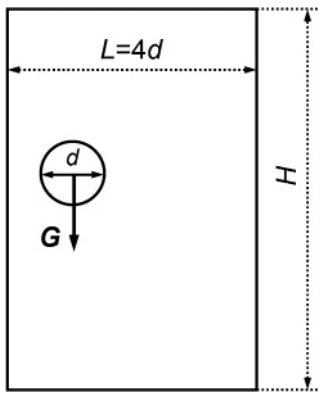

FIG. 4. Schematic diagram of cylinder sedimentation in a vertical channel, $\boldsymbol{G}$ is the gravity.

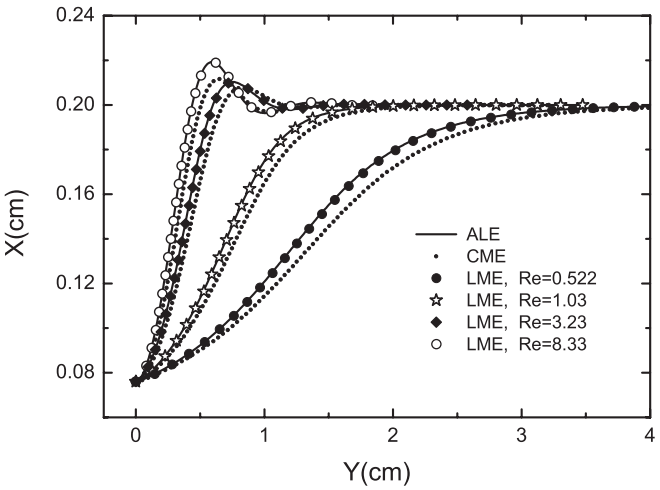

FIG. 5. Time-dependent particle trajectories at different Reynolds numbers. The real curves are the numerical results from ALE and the dotted curves are the results form CME while the symbols are the simulation results from the lattice Boltzmann method with the present momentum-exchange method.

from the left wall, and then it settles under the gravity $|\boldsymbol{G}| = 980\ \mathrm{cm}^2/\mathrm{s}$. The fluid density and its kinematic viscosity are $1\ \mathrm{g/cm}^3$ and $0.01\ \mathrm{cm}^2/\mathrm{s}$, respectively. In the present lattice Boltzmann simulations, the relaxation time τ is 0.6. The diameter of the cylinder is $d = 26$ lattice units. Thus the channel width is $L = 104$ lattice units. The channel length is set as $H = 800$ lattice units. The cylinder is placed initially at 19.76 lattice units apart from the left wall in the horizontal direction and at the middle of the channel in the vertical direction. Zero velocities are applied uniformly at the inlet and the normal derivative of the velocity is set to zero at the outlet. The translation of the mass center and the rotation of the solid particle are updated at each Newtonian dynamics time step by using a so-called half-step "leap-frog" scheme [42].

We study four cases with different fluid-solid density ratios, which are 1.0015, 1.003, 1.01, and 1.03, respectively. The terminal Reynolds numbers of the particles are 0.522, 1.03, 3.23, and 8.33 correspondingly, which is defined as $\mathrm{Re} = du_p/v$, where u_p is the final velocity of the particle. The settling trajectories at different Reynolds numbers are shown in Fig. 5, together with the simulation results from ALE and CME methods. Figures 6–8 further display the time-dependent velocities and angular velocities at different Reynolds numbers. The simulating results of LME agree with the benchmarks from ALE in a high degree of accuracy, while those of CME show some evident differences.

We have also performed the simulations of the cylinder sedimentations on MRT [45,46] with the curved boundary condition proposed by Lallemand and Luo [20]. The parameters are the same as those used above except that the relaxation parameters for MRT are set as $s_0 = 0$, $s_1 = 1.64$, $s_2 = 1.54$, $s_3 = 0$, $s_4 = 1.9$, $s_5 = 0$, $s_6 = 1.9$, $s_7 = 1/0.6$, $s_8 = 1/0.6$ (0.6 is the value of the single relaxation parameter of SRT). The LME and CME results on MRT are almost identical to their counterparts on SRT, namely Figs. 3 and 5–8. These illustrate that LME is independent of a given curved boundary condition and can be used on different lattice Boltzmann models.

B. Motion of a neutrally buoyant circular cylinder in a Poiseuille flow

Segré and Silberberg [48] reported in 1962 that neutrally buoyant particles in a pipe flow would migrate laterally away from the wall and reach a certain lateral equilibrium position.

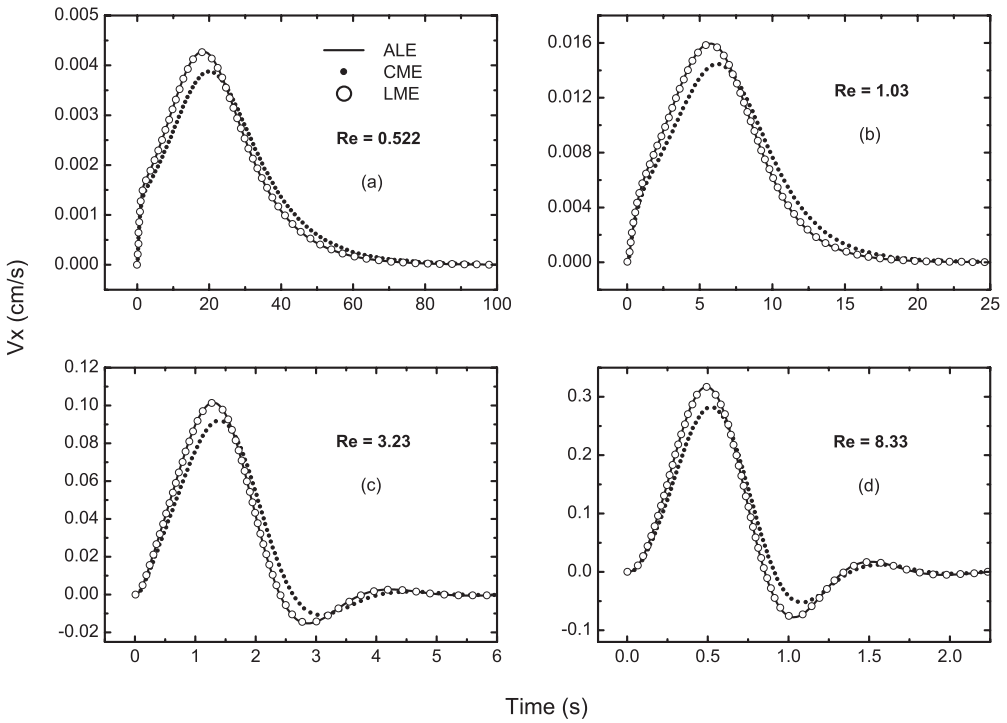

FIG. 6. Time-dependent particle velocities in horizontal direction at different Reynolds numbers.

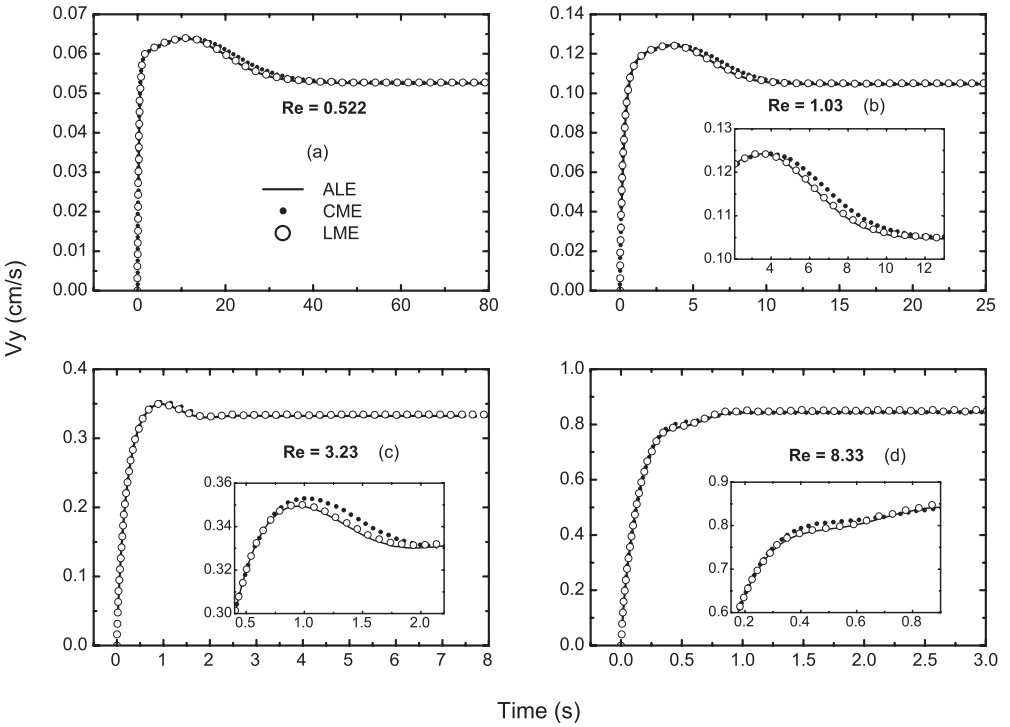

FIG. 7. Time-dependent particle velocities in vertical direction at different Reynolds numbers.

Karnis *et al.* [50] performed numerous experiments on the migrations of various particles, including spheres, rods, and disks, in a Poiseuille flow within a capillary tube. They verified that this appeared to be due to an inertia effect of the flow. Tachibana [51] found experimentally that the phenomenon was clearer when the ratio of the particle diameter to the pipe diameter exceeded 0.2. Using the lattice Boltzmann method, Inamuro *et al.* [41] and Li *et al.* [42] investigated numerically the phenomenon by the integration-stress method, and the results were consistent with the Segré-Silberberg effect. Meanwhile, Li *et al.* [42] reported that the conventional momentum-exchange method gave false trajectories of the cylinder. No matter where the cylinder was released in the tube flow, it always migrated towards the middle and finally

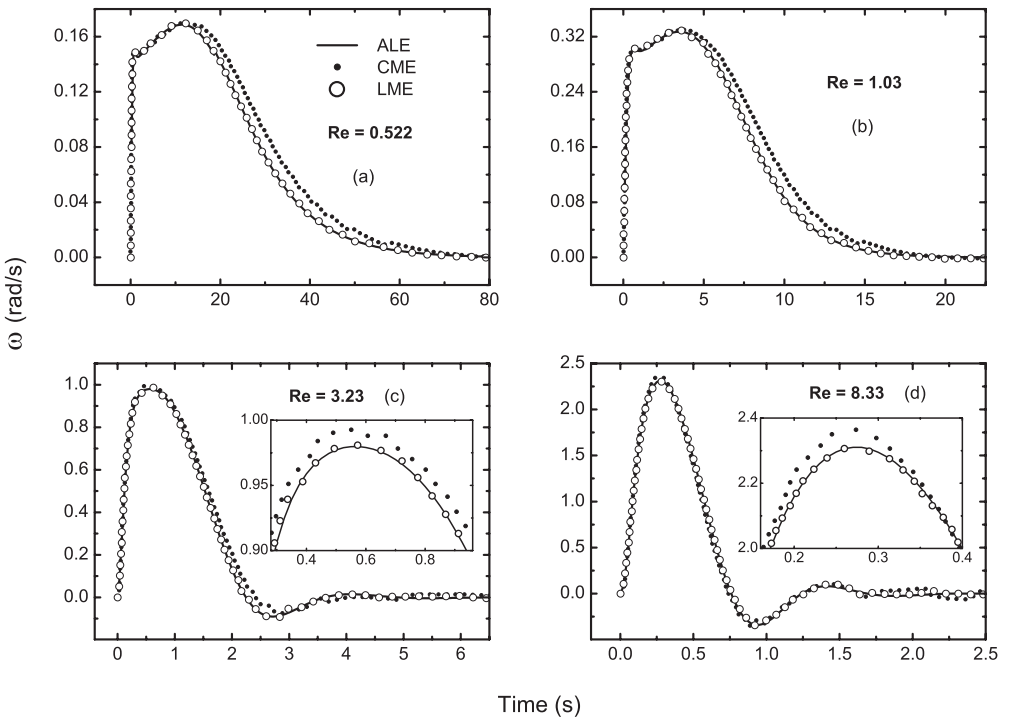

FIG. 8. Time-dependent angular velocities at different Reynolds numbers.

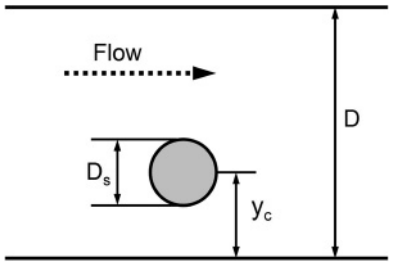

FIG. 9. Neutrally buoyant circular cylinder floating in Poiseuille flow.

stayed at the center line of the tube, if the hydrodynamics force was evaluated by the conventional method.

Figure 9 displays a schematic diagram in our lattice Boltzmann simulations of a single cylinder in a Poiseuille flow. The length of the tube is 500 lattice units and the width is $D = 100$ lattice units. The diameters of the cylinders are $D_s = 0.25D, 0.35D$ respectively. The pressure drop from the inlet to the outlet is $2\Delta p$, where $\Delta p = 2 \times 10^{-4}$. Pressure boundary conditions [52] are applied at both the inlet and outlet. The cylinder is placed initially at the middle of the tube in the horizontal direction and at $y_c/D = 0.2, 0.25, 0.35, 0.40, 0.45$ in the vertical direction, where y_c is the vertical position of the cylinder. The relaxation time is set as $\tau = 0.75$. The flow and the particle are set at rest at the beginning, and the flow evolutes and approaches steady state gradually. Then, the particle is released and moves with the fluid flow, and it reaches the lateral equilibrium position finally. The terminal Reynolds number of the Poiseuille flow is 9.6.

Our simulating results with $D_s = 25$ and $D_s = 35$ are plotted in Fig. 10. It is quite obvious that the Segré-Silberberg effect is well found in our simulations. The final equilibrium position of the cylinder with $D_s = 25$ is $y_c/D = 0.286$, which is similar to the simulated results by Inamuro *et al.* [41] and Li *et al.* [42]. The equilibrium position of the cylinder with $D_s = 35$ is $y_c/D = 0.311$, which is closer to the center line than that with $D_s = 25$. This is consistent with the observed results by Karnis *et al.* [50] and Tachibana [51] that the lateral migration of spheres in pipe flows depends mainly on the ratio of the sphere diameter to the pipe diameter, and the larger the particle is, the closer to the center line it will migrate.

VI. CONCLUSION AND DISCUSSION

We have proposed a lattice-type-dependent momentum-exchange method to evaluate the hydrodynamic forces on moving boundaries in the lattice Boltzmann simulations. Supplementing the momenta of the type-changing lattices into the conventional approach, the lattice-type-dependent momentum-exchange method obtains a high degree of accuracy in the test cases.

A series of cylinder sedimentations in a vertical tube are investigated to verify the proposed method, and the results show that the simulated time-dependent trajectories, forces, velocities, and angular velocities of the moving particles are in excellent agreement with the benchmarks from the arbitrary Lagrangian-Eulerian technique. Compared with CME, by which the cylinder in a Poiseuille flow always migrates to the center line in the simulation, the approach presented here can simulate correctly the lateral migration, and the results are consistent with the Segré-Silberberg effect as well as the previous published results. All the numerical results illustrate that the algorithm presented here can be used to evaluate accurately the hydrodynamic forces on moving boundaries.

It is important that the proposed method is independent of the boundary geometries and is easily implemented in both two and three dimensions. This offers the ability to evaluate conveniently the hydrodynamic forces on complex and moving geometries with a high level of accuracy in lattice Boltzmann simulations, which are usually hard to handle by the boundary-integration method. Finally, LME can also utilize other curved boundary conditions and can be implemented on different lattice Boltzmann models, such as SRT, MRT, TRT, etc.

ACKNOWLEDGMENTS

We thank Professor Li-Shi Luo and Professor Zhao-Li Guo for useful discussions. This work was supported by the National Science Foundation of China under Grants No. 10825520, No. 11162002, and No. 11065006, the National Basic Research Program of China under Grant No. 2012CB932400, and Shanghai Supercomputer Center of China.

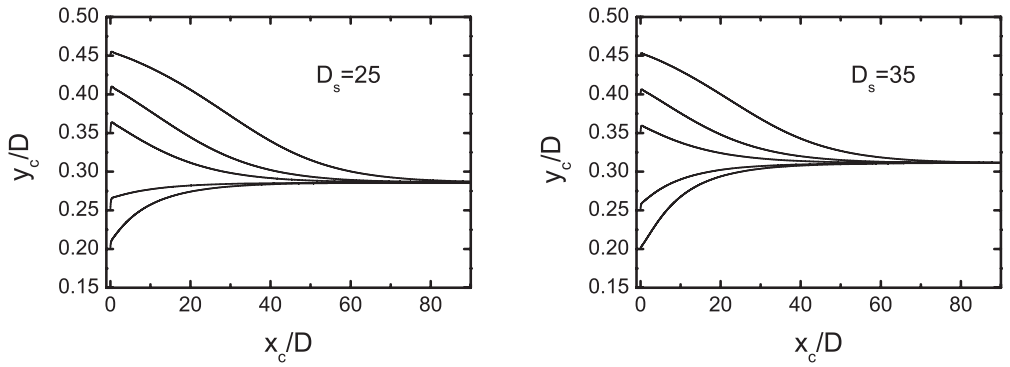

FIG. 10. Lateral migration of a cylinder from different initial positions in a Poiseuille flow with $D_s/D = 0.25, 0.35$, obtained by lattice Boltzmann method with the lattice-type-dependent momentum-exchange method at Reynolds number Re = 9.6. The final equilibrium positions of the cylinders are $y_c/D = 0.286, 0.311$.

[1] H. D. Chen, S. Y. Chen, and W. H. Matthaeus, Phys. Rev. A **45**, R5339 (1992).
[2] Y. H. Qian, D. Dhumieres, and P. Lallemand, Europhys. Lett. **17**, 479 (1992).
[3] R. Benzi, S. Succi, and M. Vergassola, Phys. Rep. **222**, 145 (1992).
[4] S. Y. Chen and G. D. Doolen, Annu. Rev. Fluid Mech. **30**, 329 (1998).
[5] C. K. Aidun and J. R. Clausen, Annu. Rev. Fluid Mech. **42**, 439 (2010).
[6] B. Dünweg and A. Ladd, Adv. Polym. Sci. **221**, 89 (2009).
[7] A. J. C. Ladd and R. Verberg, J. Stat. Phys. **104**, 1191 (2001).
[8] S. Succi, Phys. Rev. Lett. **89**, 064502 (2002).
[9] H. B. Li, H. H. Yi, X. W. Shan, and H. P. Fang, Europhys. Lett. **81**, 54002 (2008).
[10] Z. L. Guo, T. S. Zhao, and Y. Shi, J. Appl. Phys. **99**, 074903 (2006).
[11] Z. L. Guo, P. Asinari, and C. G. Zheng, Phys. Rev. E **79**, 026702 (2009).
[12] R. Benzi, L. Biferale, M. Sbragaglia, S. Succi, and F. Toschi, J. Fluid Mech. **548**, 257 (2006).
[13] X. Y. He, S. Y. Chen, and R. Y. Zhang, J. Comput. Phys. **152**, 642 (1999).
[14] J. Tölke, S. Freudiger, and M. Krafczyk, Comput. Fluids **35**, 820 (2006).
[15] S. Succi, M. Vergassola, and R. Benzi, Phys. Rev. A **43**, 4521 (1991).
[16] S. Y. Chen, H. D. Chen, D. Martinez, and W. Matthaeus, Phys. Rev. Lett. **67**, 3776 (1991).
[17] P. J. Dellar, J. Fluid Mech. **667**, 520 (2011).
[18] H. P. Fang, Z. F. Lin, and Z. W. Wang, Phys. Rev. E **57**, R25 (1998).
[19] H. P. Fang, Z. W. Wang, Z. F. Lin, and M. R. Liu, Phys. Rev. E **65**, 051925 (2002).
[20] P. Lallemand and L. S. Luo, J. Comput. Phys. **184**, 406 (2003).
[21] I. Ginzburg and D. d'Humieres, Phys. Rev. E **68**, 066614 (2003).
[22] A. J. C. Ladd, J. Fluid Mech. **271**, 285 (1994).
[23] A. J. C. Ladd, J. Fluid Mech. **271**, 311 (1994).
[24] C. K. Aidun and Y. N. Lu, J. Stat. Phys. **81**, 49 (1995).
[25] C. K. Aidun, Y. N. Lu, and E. J. Ding, J. Fluid Mech. **373**, 287 (1998).
[26] D. W. Qi and L. S. Luo, J. Fluid Mech. **477**, 201 (2003).
[27] H. B. Li, H. P. Fang, Z. F. Lin, S. X. Xu, and S. Y. Chen, Phys. Rev. E **69**, 031919 (2004).
[28] O. Behrend, Phys. Rev. E **52**, 1164 (1995).
[29] E. Lorenz, A. Caiazzo, and A. G. Hoekstra, Phys. Rev. E **79**, 036705 (2009).
[30] R. W. Mei, D. Z. Yu, W. Shyy, and L. S. Luo, Phys. Rev. E **65**, 041203 (2002).
[31] O. Filippova and D. Hanel, J. Comput. Phys. **147**, 219 (1998).
[32] R. W. Mei, L. S. Luo, and W. Shyy, J. Comput. Phys. **155**, 307 (1999).
[33] R. W. Mei, W. Shyy, D. Yu, and L. S. Luo, J. Comput. Phys. **161**, 680 (2000).
[34] A. J. C. Ladd, Phys. Rev. Lett. **76**, 1392 (1996).
[35] D. W. Qi, J. Fluid Mech. **385**, 41 (1999).
[36] R. Z. Wan, H. P. Fang, Z. F. Lin, and S. Y. Chen, Phys. Rev. E **68**, 011401 (2003).
[37] C. Y. Zhang, J. Shi, H. L. Tan, M. R. Liu, and L. J. Kong, Chin. Phys. Lett. **21**, 1108 (2004).
[38] C. Y. Zhang, H. L. Tan, M. R. Liu, L. J. Kong, and J. Shi, Chin. Phys. Lett. **22**, 896 (2005).
[39] H. Basagaoglu, P. Meakin, S. Succi, G. R. Redden, and T. R. Ginn, Phys. Rev. E **77**, 031405 (2008).
[40] X. Y. He and G. Doolen, J. Comput. Phys. **134**, 306 (1997).
[41] T. Inamuro, K. Maeba, and F. Ogino, Int. J. Multiphase Flow **26**, 1981 (2000).
[42] H. B. Li, X. Y. Lu, H. P. Fang, and Y. H. Qian, Phys. Rev. E **70**, 026701 (2004).
[43] Z. H. Xia, K. W. Connington, S. Rapaka, P. T. Yue, J. J. Feng, and S. Y. Chen, J. Fluid Mech. **625**, 249 (2009).
[44] H. H. Hu, N. A. Patankar, and M. Y. Zhu, J. Comput. Phys. **169**, 427 (2001).
[45] P. Lallemand and L. S. Luo, Phys. Rev. E **61**, 6546 (2000).
[46] L.-S. Luo, W. Liao, X. Chen, Y. Peng, and W. Zhang, Phys. Rev. E **83**, 056710 (2011).
[47] I. Ginzburg, F. Verhaeghe, and D. d'Humieres, Commun. Comput. Phys. **3**, 427 (2008).
[48] G. Segre and A. Silberberg, J. Fluid Mech. **14**, 115 (1962).
[49] J. Feng, H. H. Hu, and D. D. Joseph, J. Fluid Mech. **261**, 95 (1994).
[50] A. Karnis, H. L. Goldsmith, and S. G. Mason, Can. J. Chem. Eng. **44**, 181 (1966).
[51] M. Tachibana, Rheol. Acta **12**, 12 (1973).
[52] Q. S. Zou and X. Y. He, Phys. Fluids **9**, 1591 (1997).